LBL-29144
Preprint

Lawrence Berkeley Laboratory
UNIVERSITY OF CALIFORNIA

Materials & Chemical Sciences Division

Submitted to Journal of the American Ceramic Society

Pre-Coarsening to Improve Microstructure and Sintering of Powder Compacts

M.-Y. Chu, L.C. De Jonghe, and M.K.F. Lin

May 1990

Prepared for the U.S. Department of Energy under Contract Number DE-AC03-76SF00098.

DISCLAIMER

PRE-COARSENING TO IMPROVE MICROSTRUCTURE AND SINTERING OF POWDER COMPACTS

May-Ying Chu*, **Lutgard C. De Jonghe***, and **Mark K. F. Lin***,****,

Materials and Chemical Sciences Division

Lawrence Berkeley Laboratory

and

Department of Materials Science and Mineral Engineering

University of California,

Berkeley, CA 94720

Abstract

MgO and Al_2O_3 were sintered by two types of processes: a conventional isothermal sintering, and a two-step sintering consisting of an initial low temperature pre-coarsening treatment before conventional isothermal sintering. The final microstructure from two-step sintering is more uniform and finer than that of compacts sintered conventionally.

The differences between two-step and conventional processing are clarified by experiments in pre-coarsened and as-received ZnO powders. These compacts were pre-coarsened at 450°C for 90 hours with virtually no increase in the overall density. The resulting grain size was 1.7 times the starting one, but the standard deviation of the pre-coarsened powder size distribution was narrower than that of the as-received powder. The sintering stress of the pre-coarsened ZnO is approximately 0.8 that of the as-received one. A computational model has been used with two components of coarsening to describe the differences in pore spacing evolution between the pre-coarsened and the as-received system.

The benefit of two-step sintering is attributed to the increase in uniformity resulting from pre-coarsening. The increased uniformity decreases sintering damage and allows the system to stay in the open porosity state longer, delaying or inhibiting additional coarsening (grain growth) during the final stage of densification. Two-step sintering is especially useful for non-uniform powder systems with a wide size distribution and is a simple and convenient method of making more uniform ceramic bodies without resorting to specialized powders or complicated heat schedules.

Supported by the Division of Materials Sciences, Office of Basic Energy Sciences, U.S. Department of Energy, under contract No. DE-AC03-76SF00098.

* Member, the American Ceramic Society

** Permanent address: Institute of Nuclear Energy Research, P.O. Box 3-314, Long-Tan Tan-Yen 32500, Taiwan, R. O. C.

1 INTRODUCTION

Agglomeration is a problem common to most ceramics powders, and is well known to increase with decreasing particle size.[1] Green bodies formed from such powders contain regions of non-uniform packing, and these lead to differential densification and sintering damage. The powder compact is particularly susceptible to the development of such sintering damage in the early stages of densification since the interparticle necks are then small and can rupture easily. Direct observations of sintering damage development were reported in the work of Weiser and De Jonghe[2] on planar arrangements of uniform copper spheres, showing damage development resulting from differential densification to be most active in the earliest stages of densification.

While the development of some sintering damage is virtually unavoidable, efforts to produce more homogeneous initial powder compacts can bring considerable benefit. A number of researchers has addressed the issue of initial heterogeneity. Yan et al[3] demonstrated that by narrowing the size distribution of the powders limiting densities could be increased from 0.9 to 0.99 of theoretical. Carpay[4] found that a wide pore size distribution increases the tendency for exaggerated grain growth. Carlstrom et al[5] observed that for alpha-SiC, heterogeneities in the green body tend to remain in the system and inhibit sintering to high final densities. Numerous efforts have pursued the manipulation of the microstructure by controlling the sintering heat schedule. "Ratio control sintering"[6,7] is a process by which the relative rates of coarsening and densification are determined by the choice of the sintering temperature. For example, in the case of Al_2O_3 the activation energy for densification is higher than that for grain growth, and sintering at high temperatures is therefore indicated. For MgO, however, the relationship between grain growth and densification activation energies is uncertain, and it is therefore more difficult to specify an optimum sintering temperature. A corollary of "ratio controlled sintering" is "ultra-rapid firing"[8], which can produce dense material with fine grain size by minimizing the time spent at temperatures where grain growth is rapid compared to densification. "Rate-controlled sintering"[9], in which attempts are made to keep the densification rate constant by adjusting the temperature, in some cases has also been reported to have beneficial effects on the microstructure. These methods work best for non-agglomerated powder compacts; for agglomerated systems the benefits are less clear, and additional processing steps must be developed that could remedy, at least in part, the common heterogeneities produced during powder consolidation.

The approach in the present work has been to pre-coarsen the initial powder compact at some low temperature where little or no densification occurs. In addition to strengthening the necks between particles, thereby decreasing the risk of sintering damage development from differential densification, the powder

compacts were found to evolve towards a microstructure that is more uniform than that of the initial one. The combination of these two effects are exploited in a two-step sintering heat schedule that incorporates such pre-coarsening before firing at higher temperatures. The results of this two-step sintering are contrasted with those of a conventional firing schedule that brings the compacts directly to the final firing temperature, the single-step sintering. The materials examined initially were magnesia and alumina, while more detailed information on the consequences of pre-coarsening was derived from studies on zinc oxide.

2 EXPERIMENTAL PROCEDURES

2.1 Two-step versus single-step sintering

2.1.1 MgO

MgO* powder (diameter 6 mm by 5 mm) was compacted in a die to a green density of 0.40 ±0.01 of theoretical. This powder was also used in earlier studies,[10] and is shown in Fig. 1; it has a narrow size distribution but is agglomerated.

Conventional one-step sintering was accomplished isothermally at 1600°C for 1 hour. The sample was first heated to 850°C at 10°C/min and then heated to 1600°C at approximately 75°C/min. For two-step sintering the same MgO pellets were initially pre-coarsened at 1250°C for 48 hours and then sintered at 1600°C for one hour. The density after the 1250°C heat treatment was 0.80 ±0.01 and the final density for both single-step and two-step sintering was 0.93 ±0.01 of theoretical. Schematics of the temperature schedule for the two types of sintering are shown in Fig. 2. Fracture surfaces were examined by scanning electron microscopy (SEM). The average grain size was measured from polished sections. In addition, compacts with the same starting density were sintered isothermally at either 1500°C or 1250°C. Heating schedules were selected such that the samples could be compared at constant sintered densities. Fracture surfaces of samples at densities of 0.6, 0.7, and 0.8 of theoretical were examined by SEM.

2.1.2 Al_2O_3

Similar procedures to those for MgO were used for Al_2O_3**. Compacts were sintered at 1600°C for 1 hour. The two-step sintering schedule included a pre-coarsening treatment at 1300°C for 24 hours before sintering at 1600°C for 1 hour. The final density for both single and two-step sintering was 0.95± 0.01 of theoretical.

---

* Reagent Grade, J. T. Baker Chemical Co., Philipsburg, N. J.

** Alcoa Chemicals, Pittsburg, Pa.

2.2 ZnO

ZnO* powder (6mm in diameter by 5mm) was uniaxially compacted in a tungsten carbide die, at ~10 MPa to a green density of 0.49 ±0.01 of theoretical. The same powder was used in earlier sintering studies.[11, 12, 13] Pre-coarsening was accomplished by heating the compacts at 450°C for 90 hours, in air. The density of the pre-coarsened pellets increased to 0.50 ±0.01 during pre-coarsening. The fracture surfaces of the as-received and pre-coarsened powder compacts are shown in Figs. 3a and 3b, respectively.

Both the as-received and pre-coarsened compacts were then sintered in air, under identical conditions, in a loading dilatometer.[14] Sintering was completed with zero load or with a uniaxial load of 7 Newton, at a constant heating rate (CHR) of 8°C/min. The load of 7 Newton, corresponding to an initial stress on the compact of 0.24 MPa, was applied at 520°C when shrinkage just commenced. The experiment was stopped at 1200°C. The densification was nearly complete by 1000°C. The mass and dimensions of the samples were measured before and after sintering, and the final densities were verified using Archimedes' method. In a separate set of experiments, sintering with load was terminated at temperatures between 520°C and 1200°C, and the dimensions of these compacts were measured using a micrometer. Fracture surfaces and polished sections were examined with the SEM.

3 RESULTS

3.1 Sintering of MgO and Al_2O_3

Microstructures after a single isothermal heating at 1500°C or at 1250°C, at sintered densities of 0.6, 0.7, and 0.8 of theoretical are compared in Figs. 4, 5, and 6. At constant density, in each case the grain size of the compact sintered at 1250°C is larger than that of the compacts sintered at 1500°C. The difference in grain sizes is more dramatic as density increases. The grain structures at 0.8 density for sintering after 1600°C was not obtained but, extrapolating from the results of 1250°C and 1500°C single-step sintering, the grain size of a compact of 0.8 density sintered at 1600°C should be expected to be smaller than that sintered at 1250°C.

Microstructures of MgO and Al_2O_3 after conventional single-step sintering and after two-step sintering are shown in Figs. 7 and 8, respectively. For MgO and Al_2O_3 both single and two-step sintering processes led to the same final density, but the microstructure from the two-step process appears more uniform than that from conventional sintering. The average grain size of MgO after each step, plotted as a function of density, is shown in Fig. 9.

---

* Reagent Grade, Mallinckrodt Inc., Paris, Kentucky

3.2 As-received versus pre-coarsened ZnO

The microstructures of as-received and of pre-coarsened ZnO are shown in Figs. 3a and 3b. For the as-received ZnO, 75 particles were measured and their average size was 0.09±0.07 μm ; for the pre-coarsened sample 50 particles were measured and the average particle size increased to 0.15 μm but the standard deviation of the particle size distribution had actually **decreased** measurably to ±0.06 μm . This decrease in the standard deviation, not only in relative but also in absolute magnitude, reflects the microstructural homogenization that accompanies pre-coarsening.

Figure 10 shows the axial true strain, ϵ_z , versus temperature for the as-received and for the pre-coarsened ZnO samples sintered at a constant heating rate of 8°C/min, under zero applied stress and under an initial applied stress of 0.24 MPa. Each curve is an average of two runs under identical conditions; the reproducibility is ±1%. Results for the axial true strain, ϵ_z, versus the radial true strain, ϵ_r, for as-received and pre-coarsened ZnO samples were determined by quenching the sample from temperatures between 520 and 1200°C. These results are shown in Fig. 11; each datum point was obtained by using a different sample. The data in Fig. 11 have been converted to constant-stress conditions, corresponding to the initial stress of 0.24 MPa. To obtain data under constant-stress conditions the constant load data require a correction for dimensional changes due to densification.[12] The slopes of these lines, i.e. ϵ_z / ϵ_r, for as-received and for pre-coarsened ZnO are 1.207 and 1.270, respectively. The shrinkage of the sample sintered under no load is seen to be almost isotropic.

From Figs. 10 and 11 the sintered densities of as-received and the pre-coarsened samples are calculated. In Fig. 12 the densities of the pre-coarsened ZnO sintered under zero load or with an applied load are plotted as a function of temperature. Within the limits of experimental error, the applied load has no effect on the densification. The deformation of the sample under the action of the applied stress of 0.24 MPa is therefore constant volume creep. Both the as-received ZnO and pre-coarsened ZnO reached the same final density of 0.99 of theoretical. Also, as seen in Fig. 13, in the intermediate temperature range the density of the as-received ZnO is higher than that of the pre-coarsened ZnO.

For a body loaded uniaxially and deforming uniformly it is readily shown that the linear densification strain, ϵ_d is

$$3\epsilon_d = \epsilon_z + 2\epsilon_r \qquad \text{Eqn. 1}$$

where ϵ_d is the axial true strain and ϵ_r is the radial true strain. Correspondingly, the total axial strain, ϵ_z, is:

$$\epsilon_z = \epsilon_c + \epsilon_d \qquad \text{Eqn. 2}$$

where ϵ_c is the creep strain. It follows that

$$\epsilon_c = \frac{2}{3}(\epsilon_z - \epsilon_r) \qquad \text{Eqn. 3}$$

With Eqns. 1-3 the densification and creep strains and strain rates are found. The densification strain rates and the creep strain rates of the two types of ZnO are plotted versus temperature, in Figs. 14 and 15. In both cases the as-received ZnO starts at a higher densification and creep strain rate than the pre-coarsened sample, but later the opposite is observed.

4 DISCUSSION

The discussion has been divided into four sections. First, the effect of pre-coarsening on the sintering stress, i.e. the driving force for free sintering, is considered. Next, the effect of pre-coarsening on the evolution of the center-to-center pore spacings, x(t,T) is described for the two types of samples, based on the creep and densification data. Then, the modelling of x(t,T) is developed, and calculated and experimentally based values of x(t,T) are compared. Finally, the application of two-step sintering, i.e. pre-coarsening of powder compacts prior to densification, is discussed.

4.1 Effect of pre-coarsening on the sintering stress

The results of two-step and of single-step sintering under conditions described here should follow from an appropriate sintering and microstructural evolution model and its constitutive equations. In this paper the results will be interpreted in the context of an expression, developed earlier, for the densification and creep strain rates as well as for the microstructural evolution.

The instantaneous isothermal densification strain rate is[13]

$$\dot{\epsilon}_d = K D_o \exp\left(-\frac{Q_d}{kT}\right) \frac{\phi^{\frac{n+1}{2}}}{kT x^n} \Sigma \qquad \text{Eqn. 4}$$

where K is a constant, Σ is the sintering stress (which drives free sintering), D_o is the diffusion coefficient, Q_d is the activation energy for densification, k is Boltzman's constant, T is the absolute temperature, ϕ is the

stress intensification factor[15, 16], x is the center-to-center pore spacing (often taken as the grain size), and n is the appropriate exponent for densification, (n=2 for volume diffusion and n=3 for grain boundary diffusion, n=2 for ZnO[11]).

Under conditions of low applied stress, where the uniaxially applied stress induces creep without increasing the overall density, the mechanism for densification and creep are intimately related.[17] As evident in the plot of density versus temperature for ZnO sintered with or without an applied stress (Fig. 12) the resulting densities are identical. The creep strain rate, superimposed on the densification strain rate, is then:

$$\dot{\epsilon}_c = K_c D_o \exp\left(-\frac{Q_d}{kT}\right)\frac{\phi^{\frac{n+1}{2}}}{kT x^n}\sigma \qquad \text{Eqn. 5}$$

where K_c is a constant and σ is the uniaxially applied stress.

The relative magnitude of free-sintering driving force for the systems can be obtained from the ratio of the densification strain rate over the creep strain rate

$$\frac{\dot{\epsilon}_d}{\dot{\epsilon}_c} \propto \left(\frac{\Sigma}{\sigma}\right) \qquad \text{Eqn. 6}$$

From results of the constant-stress creep and densification the sintering stress of the pre-coarsened* sample, Σ_c, is found to be about 0.8 of the sintering stress for the as-received sample, Σ.

As coarsening proceeds , for a self-similar system a reduction in the driving force should be expected proportional to the inverse of its scale factor. Here, the average initial particle size of the pre-coarsened sample is approximately 1.7 times larger than that of the as-received sample. If the sintering stress strictly scales to the inverse of the mean particle size then one would expect Σ_c to be 0.59 of Σ. The change in the magnitude of Σ is not as large here; the difference could be due to other structural terms that arise in systems that are not strictly self-similar, such as a decrease in the average pore coordination number[18] which could increase the sintering stress.

4.2 Effect of pre-coarsening on the evolution of the center-to-center pore spacing, x(t,T)

As evident from the resulting microstucture of MgO and Al_2O_3 the two-step sintering process produced finer and more uniform grain structure than conventional single-step sintering. Due to temperature limitation

* The extra subscript "c" will denote the coarsened sample.

of the dilatometer, sintering data to full density were not obtained for MgO and Al_2O_3. However, since the behavior of as-received and pre-coarsened ZnO corresponds in many aspects to single-step and two-step sintering, the ZnO data can give insight into the origin of the microstructural differences following the two treatments for MgO and Al_2O_3.

While the two types of heat treatment for the ZnO contain the essential elements of those for the MgO and Al_2O_3 system, there are two main differences. First, a constant heating rate rather than isothermal sintering is used. CHR allows for a more precise analysis of the data, since isothermal sintering does necessarily contain a heat-up and is actually a more involved heat treatment. In addition, CHR conditions access a wider range of sintered densities. Second, during the pre-coarsening of MgO and Al_2O_3 compacts there was significant densification, in contrast to the ZnO which showed virtually no increase in density during pre-coarsening.

The relative differences in the evolution of the center-to-center pore spacing, x(t,T), between the as-received and pre-coarsened samples can be extracted from the corresponding densification strain rates. The ratio of the densification strain rate of the as-received sample over the pre-coarsened sample at any temperature follows from Eqn. 1:

$$\frac{\dot{\epsilon}_{cd}}{\dot{\epsilon}_{d}} = \left(\frac{\phi_c}{\phi}\right)^{\frac{n+1}{2}} \left(\frac{x}{x_c}\right)^{n} \left(\frac{\Sigma_c}{\Sigma}\right) \qquad \text{Eqn. 7}$$

With the experimental ratios of $\Sigma_c / \Sigma = 0.8$ and $\dot{\epsilon}_{cd} / \dot{\epsilon}_{d}$, and when the stress intensification factors for the as-received and the pre-coarsened samples have been determined from the densities at that temperature, $(x/x_c)^n$ can be found from Eqn. 7. Since ϕ is proportional to exp(aP),[19] where *a* equals 5,[11] and P is the porosity, the values of ϕ and ϕ_c are determined.

The ratio of the center-to-center pore spacings, $(x/x_c)^n$, of the as-received over the pre-coarsened ZnO is plotted versus temperature in Fig. 16. The figure is divided into a lower region where $(x/x_c) < 1$, and an upper region where $(x/x_c) > 1$. As seen in the figure, for most of the temperature range the center-to-center pore spacing of the pre-coarsened ZnO is larger than that of the as-received ZnO. However, as the temperature increases, the ratio of (x/x_c) increases steadily. At approximately 890°C where the densities of the as-received and pre-coarsened samples are approximately 0.9 of theoretical, the center-to-center pore spacing ratio crosses into the upper region where the spacing of the pre-coarsened sample now remains smaller than that of the as-received sample.

The relative lag in pore spacing increase in the pre-coarsened ZnO is only evident in the later stages of sintering. This behavior is also present in MgO samples, where at 0.8 density the grain size of the conventionally sintered sample is smaller than that of the pre-coarsened sample but later, at 0.93 density, the grain size of the two-step sintered sample is actually smaller than that of the single-step sintered sample.

4.3 Modelling of the evolution of the interpore spacing, x(t,T)

In a previous study of coarsening at constant heating rate, an expression for the evolution of the interpore spacing, x(t,T) was developed.[13] The form of the expression was taken to be analogous to that describing grain growth in porous systems, although it must be stressed that the pore spacing, x(t,T) and the grain size do not necessarily develop proportionately. The expression for the pore spacing evolution, x(t,T), the parameter of importance in Eqn. 4, recognizes two contributions to pore spacing increase: those arising from non-densifying processes and those arising from densifying processes. At constant heating rate with

$$T = T_o + \alpha t \qquad \text{Eqn. 9}$$

and

$$dT = \alpha dt \qquad \text{Eqn. 10}$$

the pore spacing relationship during densification takes the following form:

$$x^m(T) = x_o^m + \frac{A_o}{\alpha}\int_{To}^{T} \exp\left(-\frac{Q_l}{kT}\right)dT + \frac{B_o}{\alpha}\int_{To}^{T} \exp\left(-\frac{Q_h}{kT}\right)dT \qquad \text{Eqn. 12}$$

where x_o, is the starting center-to-center pore spacing at T_o, m is the coarsening exponent (m=3 for ZnO[11]), α is the heating rate, A_o is the low temperature prefactor associated with low activation energy processes, Q_l is the low activation energy, B_o is the high temperature prefactor associated with high activation energy processes, and Q_h is the high activation energy.

While the detailed relationship of this expression to the actual micro-processes has yet to be established, it could describe the evolution of x(t,T) well, and can at least lend itself to some qualitative predictions. For example, if evaporation-condensation or surface diffusional transport is a coarsening mechanism, it can only be active as long as a continuous pore network exists and will gain in importance with increasing pore channel size.[20] This would increase the magnitude of A_o with respect to B_o, where Q_l corresponds to that coarsening mechanism.

For the numerical calculation of the relative evolution of the pore spacing in the pre-coarsened compared to the as-received ZnO, the same parameters were used as determined earlier*.[13] The ratio $(x/x_c)^m$ can then be determined with $x_{co} = 1.7x_o$ appropriate to the present data.

$$\left(\frac{x}{x_c}\right)^m = \frac{x_o^m + \frac{A_o}{\alpha}\int_{To}^{T}\exp\left(-\frac{Q_l}{kT}\right)dT + \frac{B_o}{\alpha}\int_{To}^{T}\exp\left(-\frac{Q_h}{kT}\right)dT}{x_{co}^m + \frac{A_{co}}{\alpha}\int_{To}^{T}\exp\left(-\frac{Q_l}{kT}\right)dT + \frac{B_{co}}{\alpha}\int_{To}^{T}\exp\left(-\frac{Q_h}{kT}\right)dT} \quad \text{Eqn. 13}$$

The choice of A_{co} and B_{co} in Eqn. 13 must then now be such that the evolution of the calculated ratio reflects, at least qualitatively, the experimental one. Since significant coarsening had been found to occur at relatively low temperatures for this ZnO powder (CHR), the trend of the experimental ratio $(x/x_c)^n$ up to about 890°C (corresponding to a sintered density of about 0.9 of theoretical), can only be reproduced if $A_{co} > A_o$. The subsequent increase of the experimental $(x/x_c)^n$ to values higher than 1 can only result if $B_{co} < B_o$. Different choices for these parameters and calculated trends are illustrated in Fig. 17.

The effects of pre-coarsening on the evolution of the pore spacing can therefore be summarized as facilitating the low temperature coarsening but suppressing the high temperature coarsening.

4.4 Application of pre-coarsening and two-step sintering

The results of the present study can be put in the context of the qualitative evolution of porosity and grain size distributions. It should be expected that any system will strive towards the steady state distribution described by the theories of Slyozov & Lifshitz,[21] and Wagner[22] (LSW). The initial distribution of pore sizes and grain sizes and the relative importance of coarsening and densification of the compact will determine at which sintered density and mean grain size or mean pore spacing this steady state distribution is reached. Technical powders and compacts, such as the ones examined here, will most often have a structural distribution that is significantly broader than the LSW distribution; for monosized powder systems, the opposite is the case. There is therefore no merit in pre-coarsening those systems that have a structural distribution equal to or narrower than the LSW one. However, for technical powder compacts, the present results demonstrate that pre-coarsening will improve the structural distribution. Immediate densification of the compact before homogenization is likely to result in the production of sintering damage driven by differential densification, leading to the view that such immediate densification delays reaching the LSW distribution. At

---

* $A_o = 5.6 \times 10^{-9}$
$B_o = 1.0 \times 10^{0}$
$Q_l = 15$ kcal/mole
$Q_h = 50$ kcal/mole

the same time, heterogeneity promotes the generation of mixtures of open and closed porosity regions at sintered densities lower than those of more homogeneous systems, as would follow from the work of Carpay[4]. A qualitative limit on pre-coarsening must, however, be immediately recognized: if the initial distribution is too far removed from the LSW distribution then pre-coarsening needed to reach the LSW distribution would be so extensive that the mean value of x would have to be so large as to inhibit further densification. Quantitative limits on distributions are more difficult to determine, especially since clear definitions or quantitative measurements of relevant "heterogeneity" have yet to be formulated.

In practice, the usefulness of the proposed two-step sintering process is readily evaluated by a few trial experiments. The results of the experiments presented also indicate that, within limits, technical powders can be used effectively by including a simple isothermal pre-coarsening treatment and produce improved microstructures in sintered bodies without resorting to the use of monosized powders or convoluted heat schedules.

5 SUMMARY

MgO and Al_2O_3 were sintered by two types of processes: a conventional isothermal sintering, and a two-step sintering with an initial low temperature pre-coarsening treatment before conventional isothermal sintering. The final microstructure from two-step sintering is more uniform and finer than that of compacts sintered conventionally.

ZnO compacts were pre-coarsened at 450°C for 90 hours, the resulting grain size was 1.7 times larger than the starting grain size, but the standard deviation of the grain size distribution was narrower than that of the as-received powder. The pre-coarsening was completed with virtually no increase in the overall density for the ZnO compacts. Σ_c, the sintering stress of the pre-coarsened ZnO, is approximately 0.8 of the sintering stress of the as-received ZnO, Σ, decreasing less than expected from the grain size increase.

As a function of temperature the densification and creep strain rates of the pre-coarsened sample started out lower than that of the as-received sample but increased steadily as sintering proceeded, until the strain rate of the pre-coarsened sample exceeded that of the as-received sample.

A computational model has been used with two components of coarsening to describe the pore spacing evolution, one with a low activation energy and the other with a high activation energy. Pre-coarsening increases the low temperature prefactor but decreases the high temperature prefactor. This behavior has been attributed to the increase in uniformity as a resulting from pre-coarsening. The increased uniformity allows the system to stay in the open porosity state longer, delaying or inhibiting additional coarsening (grain growth) during the final stage of densification.

The benefit of two-step sintering is especially useful for non-uniform powder systems with size distributions that is wider than the LSW one. The process, incorporating an initial low temperature pre-coarsening treatment prior to densification, offers a simple and convenient method of making more uniform ceramic bodies without resorting to specialized powders or complicated heat schedules.

REFERENCES

1. W.H. Rhodes, "Agglomerate and Particle Size Effects on Sintering Yttria-Stablized Zirconia," *J. Am. Ceram. Soc.*, **64** [1] 19-22 (1981).
2. M.W. Weiser and L.C. De Jonghe, "Rearrangement During Sintering in Two-Dimensional Array," *J. Am. Ceram. Soc.*, **69** [11] 822-26 (1986).
3. M.F. Yan, R.M. Cannon, Jr., H.K. Bowen, and U. Chowdhry, " Effect of Grain Size Distribution on Sintered Density," *Mat. Sci. and Eng.*, **60** 275-81 (1983).
4. F.M.A. Carpay, "The Effect of Pore Drag on Ceramic Microstructure," in *Ceramic Microstructure '76,* ed. R. M. Fulrath and J. A. Pask (Westview Press, Colorado, 1977) p. 261-75.
5. E. Carlstrom, A.-K. Tjernlund, L. Hermansson, and R. Carlsson, "Influence of Powder and Green Compact Characteristics on Microstructure of Sintered Alpha-SiC," *Proc. Brit. Ceram. Soc.*, **33** 89-100 (1983).
6. R.J. Brook, "Fabrication Principles for the Production of Ceramics with Superior Mechanical Properties," *Proc. Brit. Ceram. Soc.*, **32** 7-24 (1982).
7. H. Pickup, U. Eisele, E. Gilbart and R.J. Brook, "Analysis of Coarsening and Densification Kinetics during the Heat Treatment of Nitrogen Ceramics," in *Non-Oxide Technical and Engineering Ceramics,* ed. S. Hampshire (Elsevier Applied Science, New York, 1985) p. 41-51.
8. D. L. Johnson, "Ultra-Rapid Sintering", *Materials Science Research Vol. 16,* ed. G. C. Kuczynski, A. E. Miller and G. A. Sargent (Plenum Press, New York, 1984) p. 243-52.
9. H. Palmour III and D.R. Johnson, "Phenomenological Model for Rate-Controlled Sintering," in *Sintering and Related Phenomena,* ed. G.C. Kuczynski, N.A. Hooton, and C.F. Gibbon (Gordon and Breach Science, New York, 1967) p. 777-92.
10. M. Lin, M.N. Rahaman, and L.C. De Jonghe, "Creep-Sintering and Microstructure Development of Heterogeneous MgO Compacts," *J. Am. Ceram. Soc.*, **70** [5] 360-66 (1987).
11. M.N. Rahaman, L.C. De Jonghe, "Creep-Sintering of Zinc Oxide," *J. Mater. Sci.*, **22** 4326-30 (1987).
12. M.-Y. Chu, L.C. De Jonghe, and M.N. Rahaman, "Effect of Temperature on the Densification/Creep Viscosity During Sintering," *Acta. metall.*, **37** [5] 1414-20 (1989).
13. M.-Y. Chu, M.N. Rahaman, and L.C. De Jonghe, "Effect of Heating Rate on Sintering and Coarsening," submitted *J. Am. Ceram. Soc.*, 1990.
14. L.C. De Jonghe and M.N. Rahaman, "Loading Dilatometer," *Rev. Sci. Instrum.* **55** [12] 2007-10 (1984).
15. W. Beere, "The Second Stage Sintering Kinetics of Powder Compacts," *Acta metall.*, **23** [1] 139-45 (1975).
16. W. Beere, "A Unifying Theory of the Stability of Penetrating Liquid Phases and Sintering Pores," *Acta metall.*, **23** [1] 131-38 (1975).
17. M.N. Rahaman, and L.C. De Jonghe, "Sintering of CdO Under Low Applied Stress," *J. Am. Ceram. Soc.*, **67** [10] C-205–07 (1984).
18. B.J. Kellet and F.F. Lange, "Thermodynamics of Densification: I, Sintering of Simple Particle Arrays, Equilibrium Configurations, Pore Stability, and Shrinkage," *J. Am. Ceram. Soc.*, **72** [5] 725-34 (1989).
19. J.M. Vieira, R.J. Brook, "Kinetics of Hot-Pressing: The Semilogarithmic Law," *J. Am. Ceram. Soc.*, **67** [4] 245-49 (1984).
20. C. Herring, "Effect of Change of Scale on Sintering Phenomena," *J. Appl. Phys.*, **21** 301-03 (1950).
21. I.M. Lifshitz and V.V. Slyozov, "The Kinetics of Precipitation from Supersaturated Solid Solutions," *Phys. Chem. Solids* **19** [1/2] 35-50 (1961).
22. C. Wagner, "Theorie der Alterung von Niederschlagen durch Umlosen (Ostwald-Reifung), *Zeitschrift fur Elektrochemie* **65** [7/8] 581-91 (1961).

FIGURE CAPTIONS

Fig. 1 Scanning electron micrograph of a fracture surface of a MgO initial compact.

Fig. 2 Schematic time-temperature heating schedules of conventional "isothermal" sintering and of two-step sintering.

Fig. 3 Scanning electron micrographs of fracture surfaces of ZnO compacts. (a) Initial compact of as-received ZnO, density of 0.49 of theoretical. (b) Compact after pre-coarsening treatment to a density of 0.50 of theoretical.

Fig. 4 Scanning electron micrographs of fracture surfaces of MgO compacts sintered to a density of 0.60 of theoretical. (a) After isothermal at 1500^{o}C. (b) After isothermal sintering at 1250^{o}C.

Fig. 5 Scanning electron micrographs of fracture surfaces of MgO compacts sintered to a density of 0.70 of theoretical. (a) After isothermal sintering at 1500^{o}C. (b) After isothermal sintering at 1250^{o}C.

Fig. 6 Scanning electron micrographs of fracture surfaces of MgO compacts sintered to a density of 0.80 of theoretical. (a) After isothermal sintering at 1500^{o}C. (b) After isothermal sintering at 1250^{o}C.

Fig. 7 Scanning electron micrographs of fractured surfaces of MgO compacts. (a) Initial compact microstructure, density of 0.40 of theoretical density. (b) Microstucture after isothermal sintering to a density of 0.93 of theoretical. (c) Microstucture after pre-coarsening treatment to a density of 0.80 of theoretical. (d) Microstructure after two-step sintering to a density of 0.93 of theoretical.

Fig. 8 Scanning electron micrographs of fractured surfaces of Al_2O_3 compacts. (a) Initial compact microstructure, density of 0.53 of theoretical. (b) Microstucture after isothermal sintering to a density of 0.93 of theoretical. (c) Microstucture after pre-coarsening treatment to a density of 0.83 of theoretical. (d) Microstructure after two-step sintering to a density of 0.95 of theoretical.

Fig. 9 Average grain sizes versus density plot for conventionally sintered and for two-step sintered MgO.

Fig. 10 Axial true strain versus temperature for as-received and for pre-coarsened ZnO.

Fig. 11 Axial true strain versus radial true strain for as-received and for pre-coarsened ZnO.

Fig. 12 Density versus temperature for pre-coarsened ZnO sintered without load and sintered with load

Fig. 13 Density versus temperature for as-received and for pre-coarsened ZnO.

Fig. 14 Densification strain rate versus temperature for as-received and for pre-coarsened ZnO.

Fig. 15 Creep strain rate versus temperature for as-received and for pre-coarsened ZnO.

Fig. 16 Ratio of the pore spacing of the as-received ZnO, x, over the pore spacing of the pre-coarsened ZnO, x_c, versus temperature, derived from dilatometry data.

Fig. 17 Ratio of the pore spacing of the as-received ZnO, x, over the pore spacing of the pre-coarsened ZnO, x_c, versus temperature from numerical calculations with the various indicated choices of parameters.

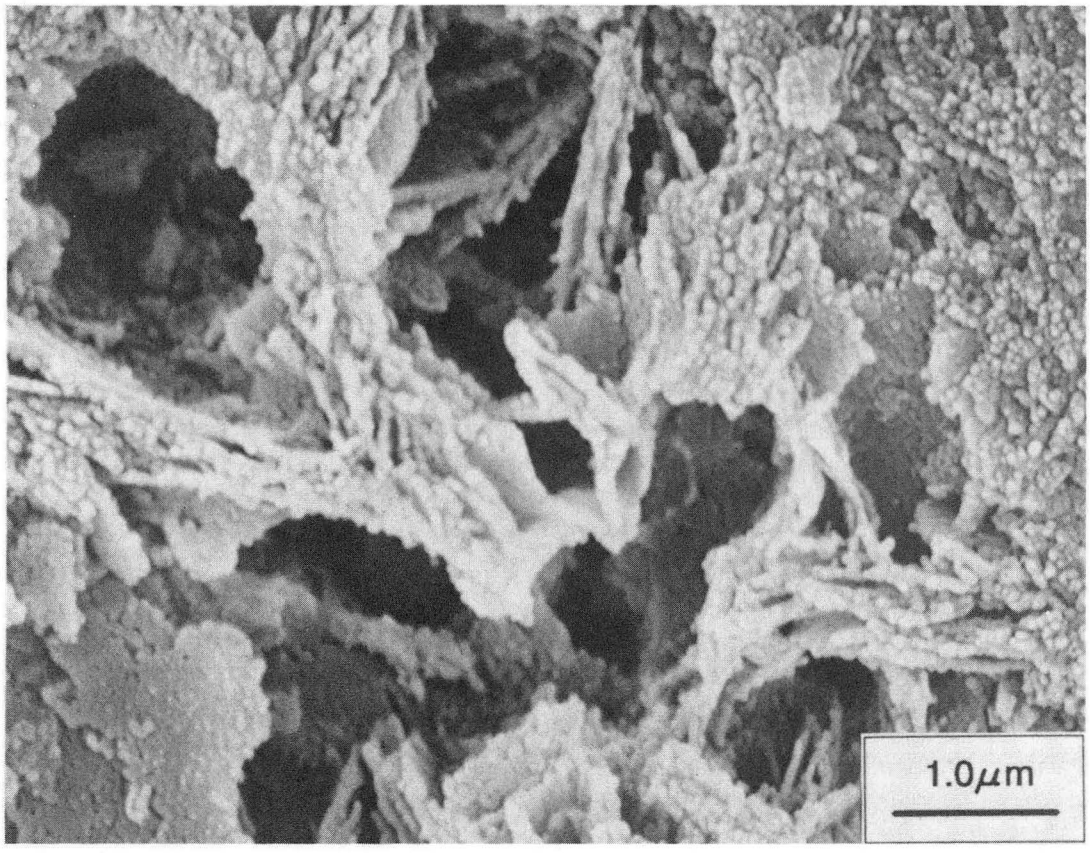

XBB 905-4310

Fig. 1

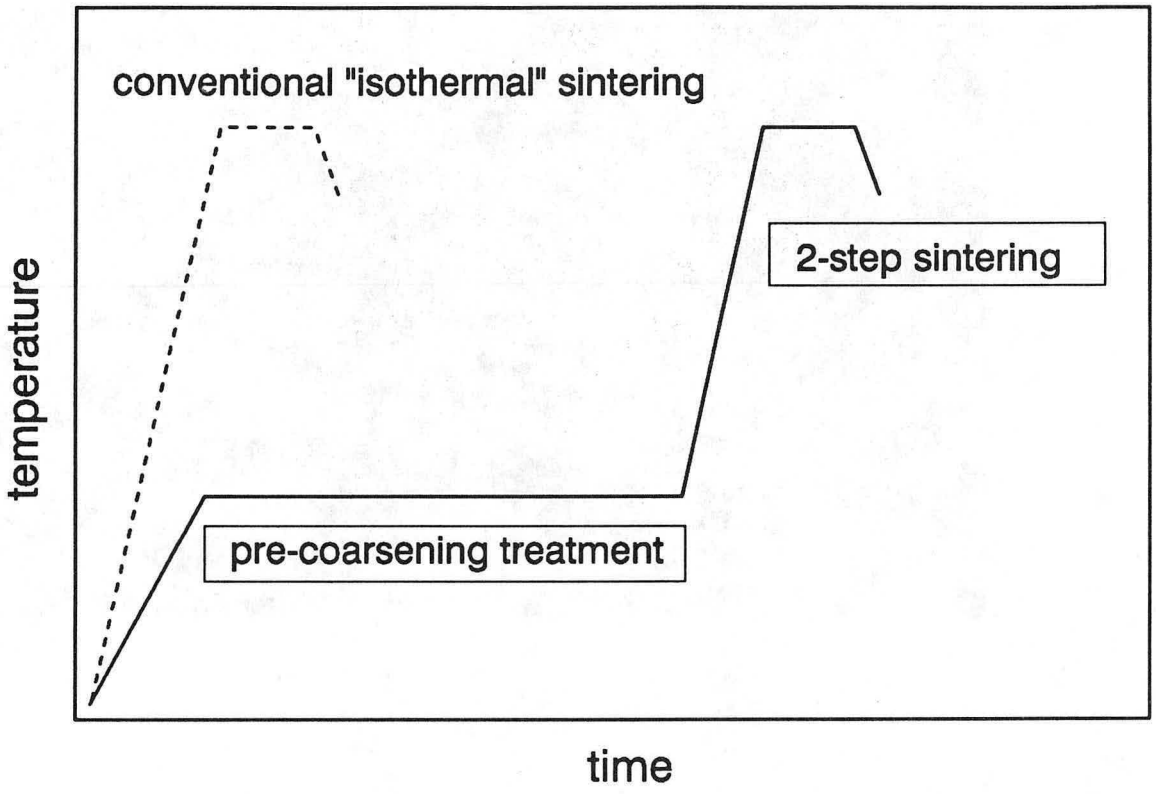

XBL 905-1899

Fig. 2

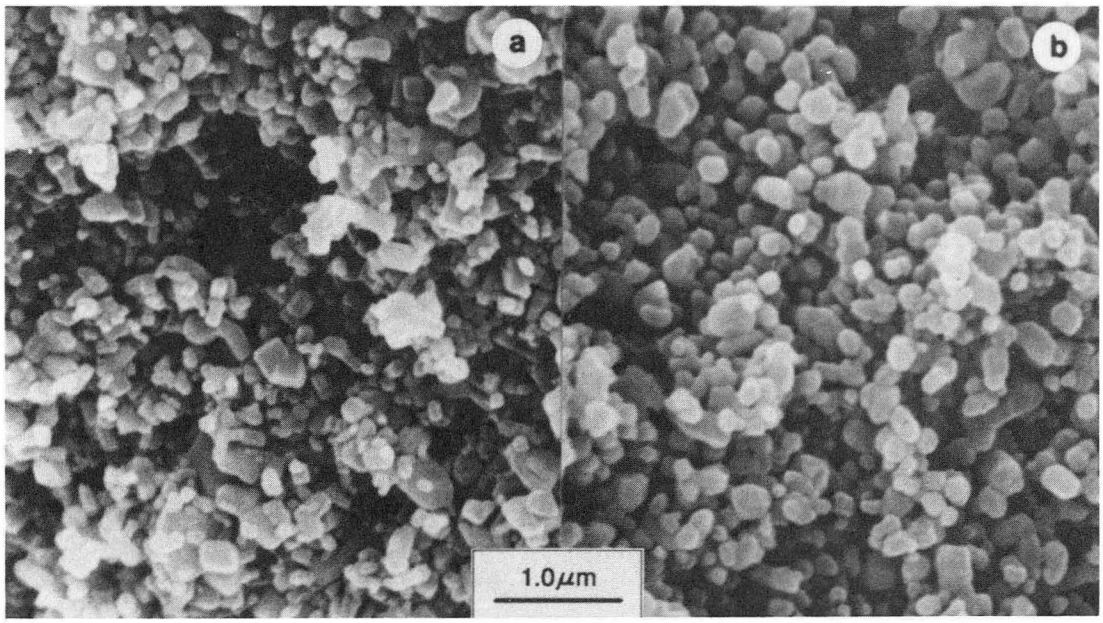

XBB 905-4309

Fig. 3

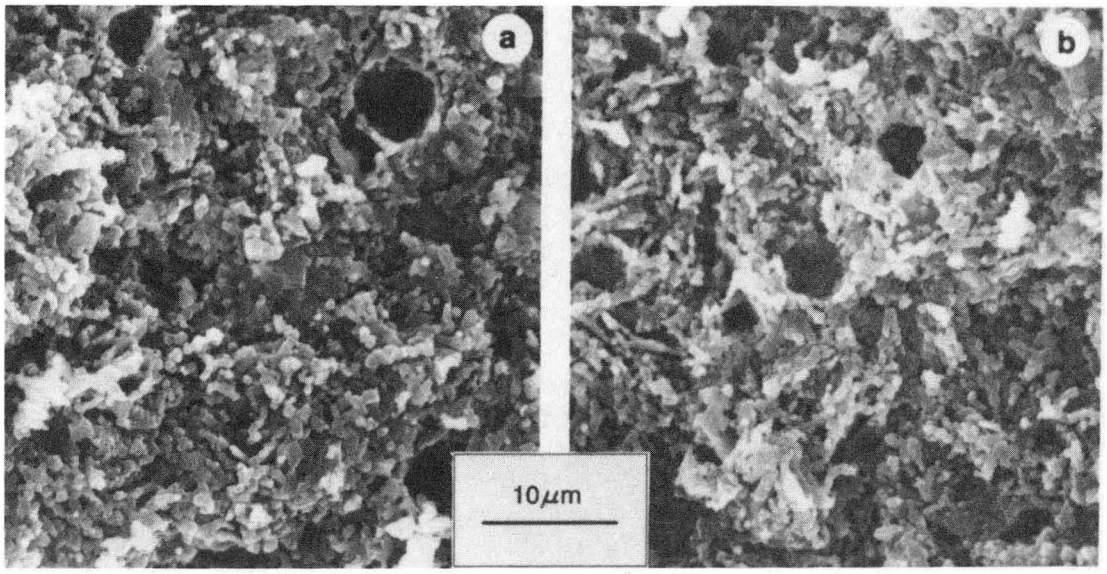

XBB 905-4308

Fig. 4

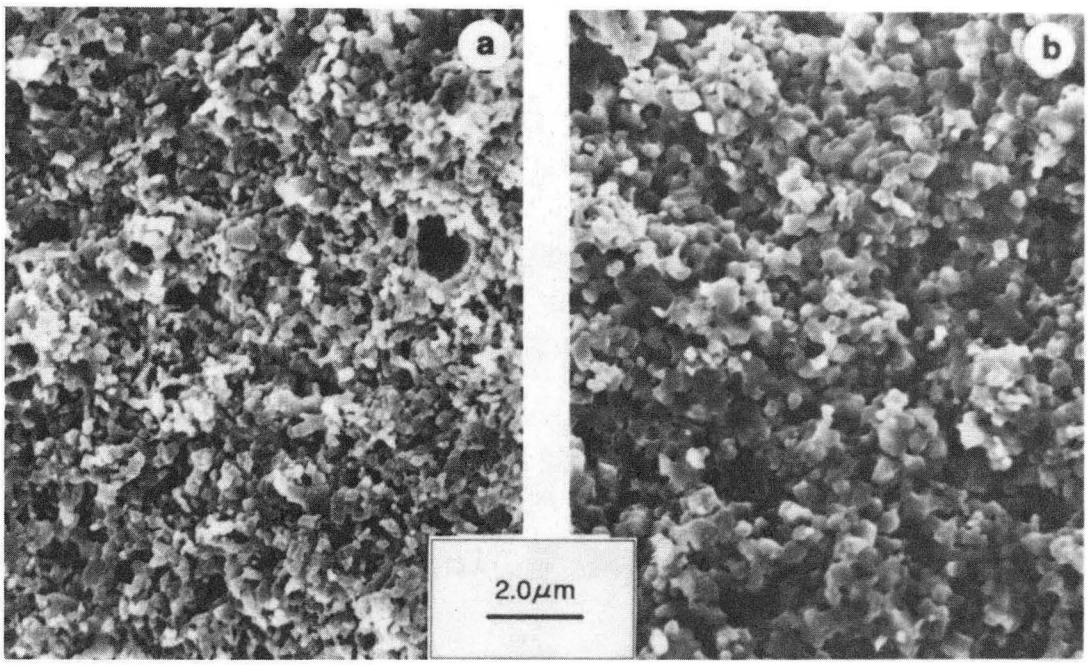

XBB 905 4307

Fig. 5

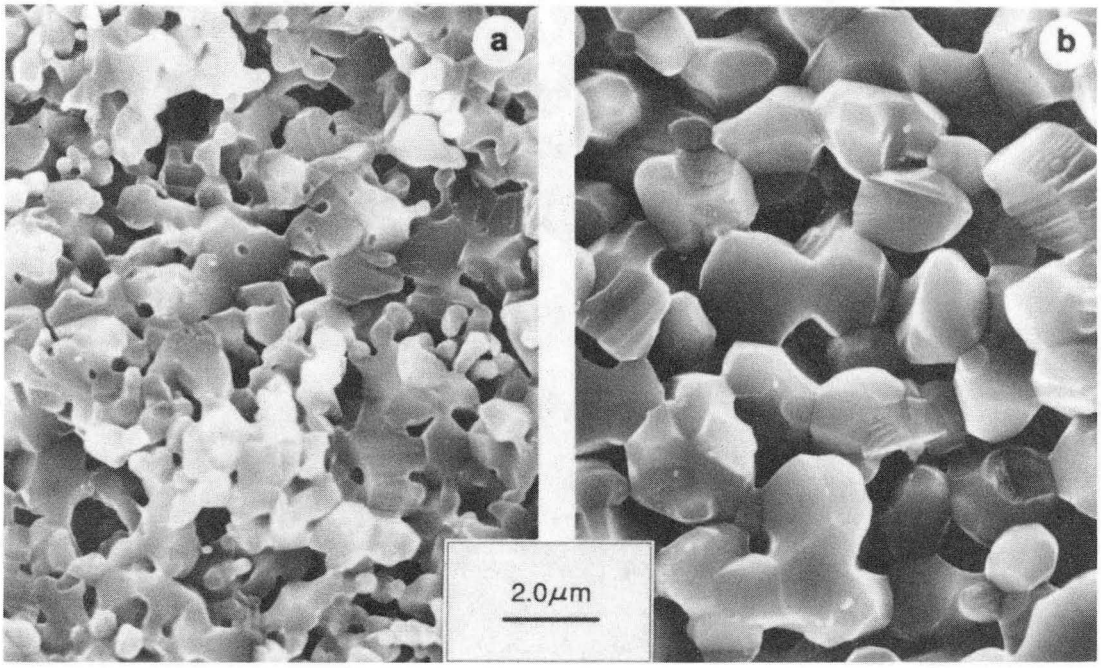

XBB 905 4306

Fig. 6

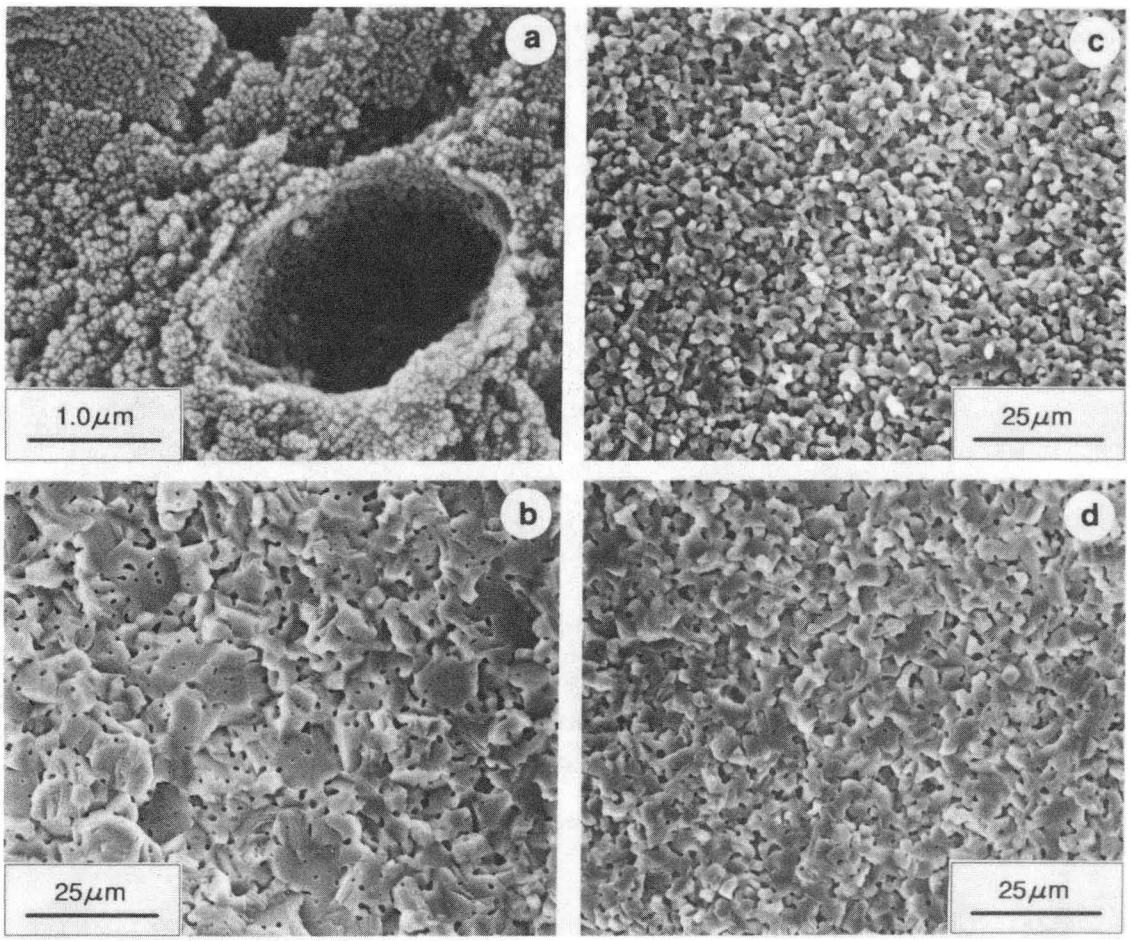

XBB 872-1440C

Fig. 7

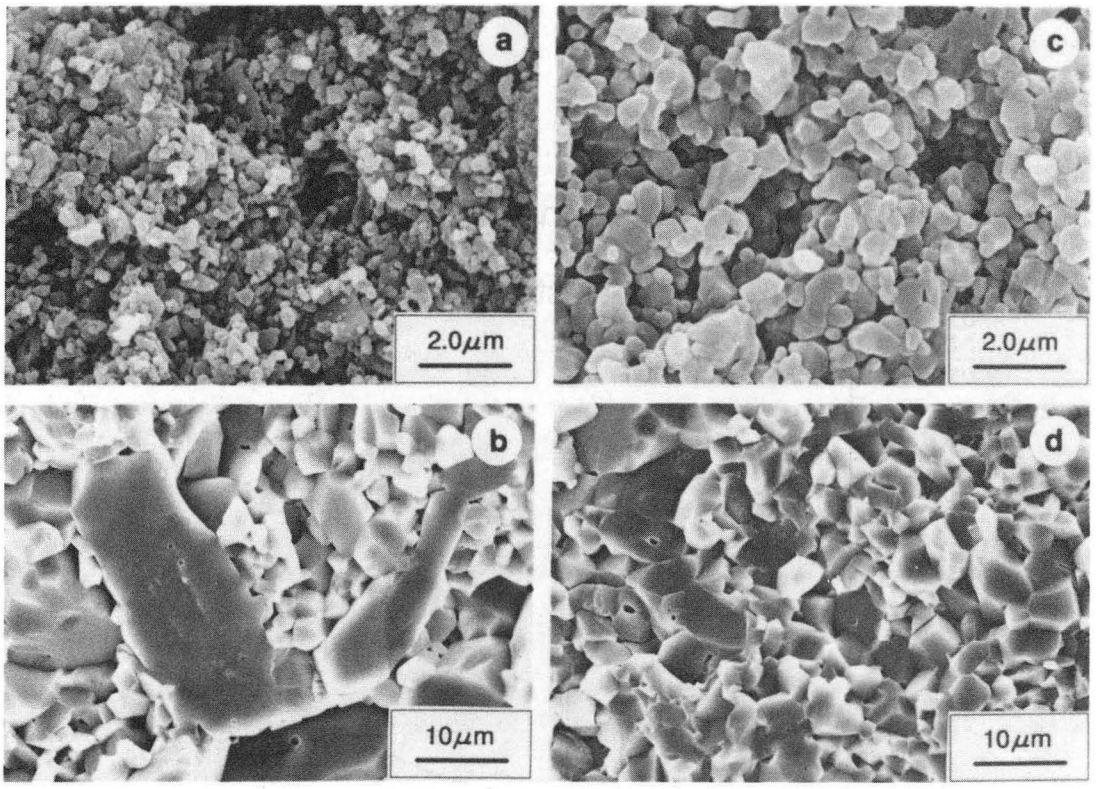

XBB 905-4305

Fig. 8

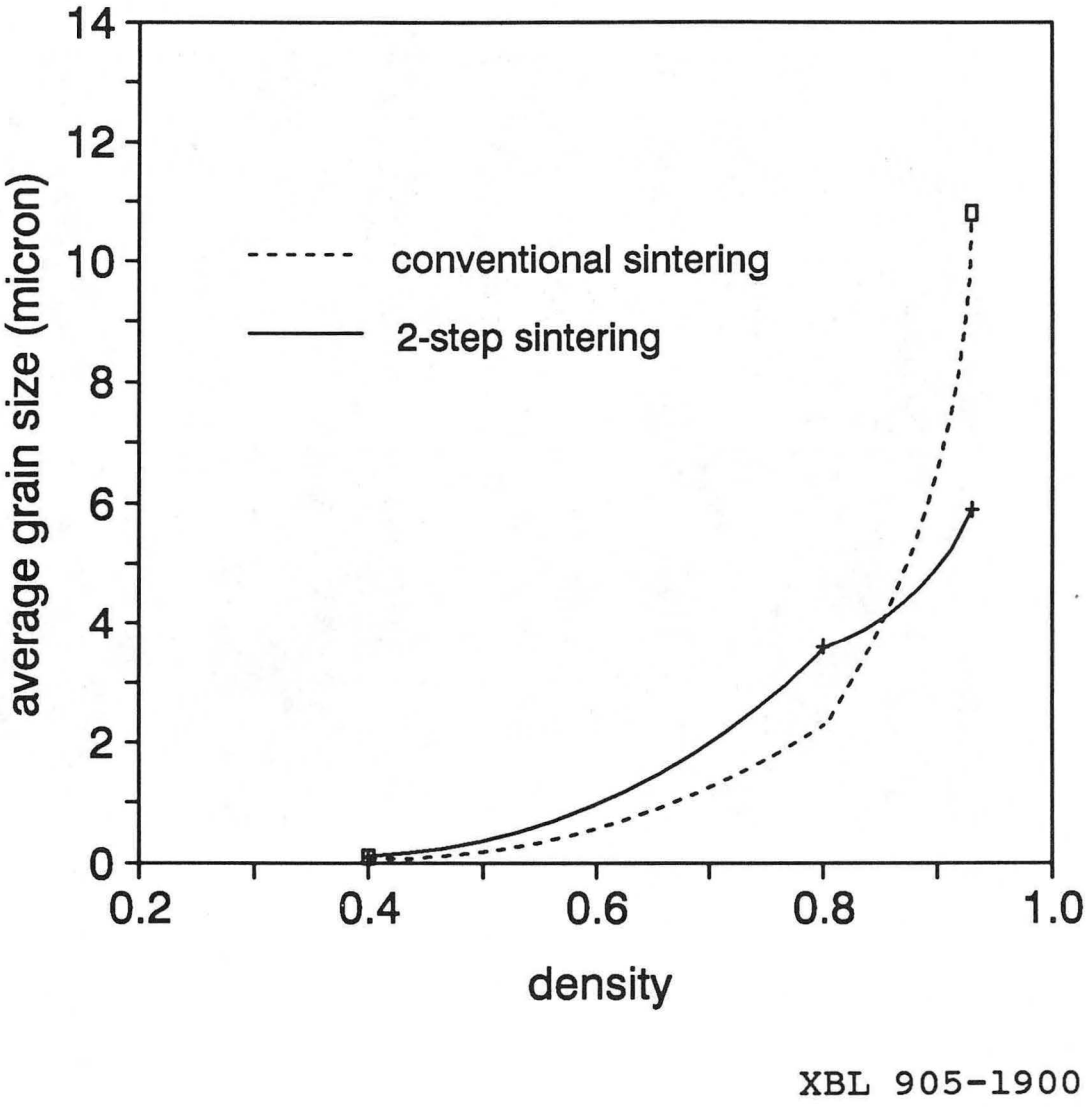
14
12
10
8
6
4
2
0
average grain size (micron)
conventional sintering
2-step sintering
0.2
0.4
0.6
0.8
1.0
density
XBL 905-1900

Fig. 9

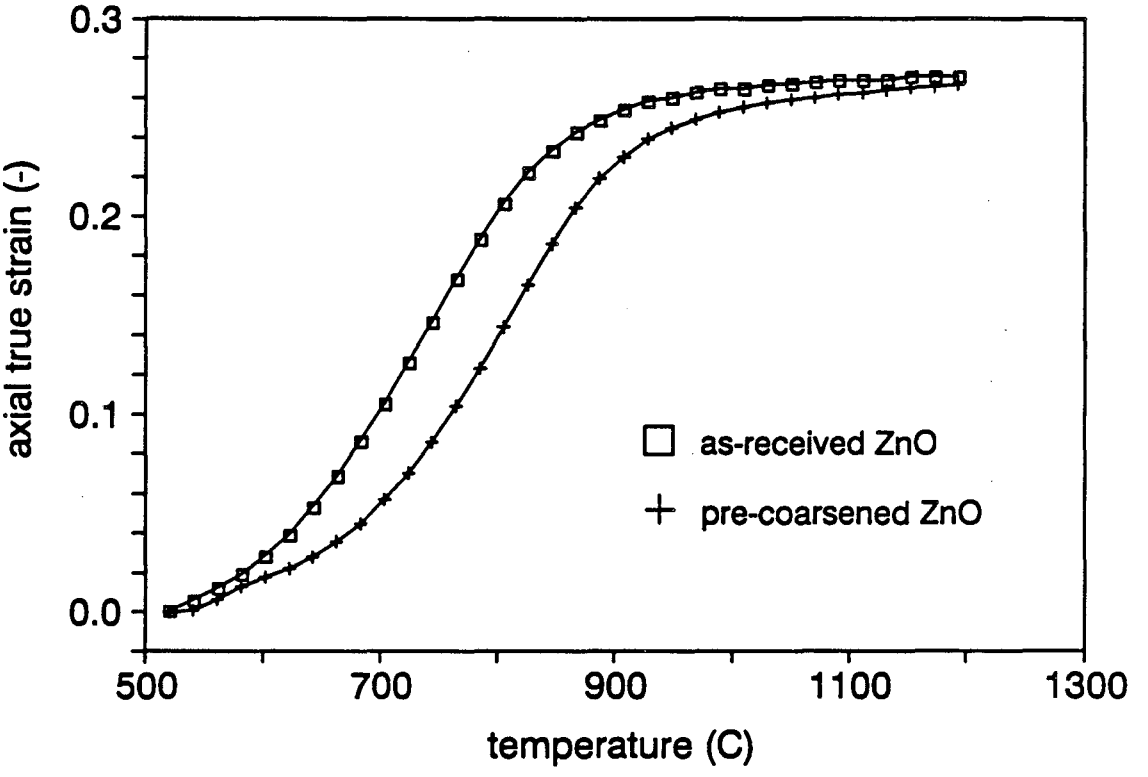
0.3
0.2
0.1
0.0
axial true strain (-)
500
700
900
1100
1300
temperature (C)
as-received ZnO
pre-coarsened ZnO
XBL 905-1901

Fig. 10

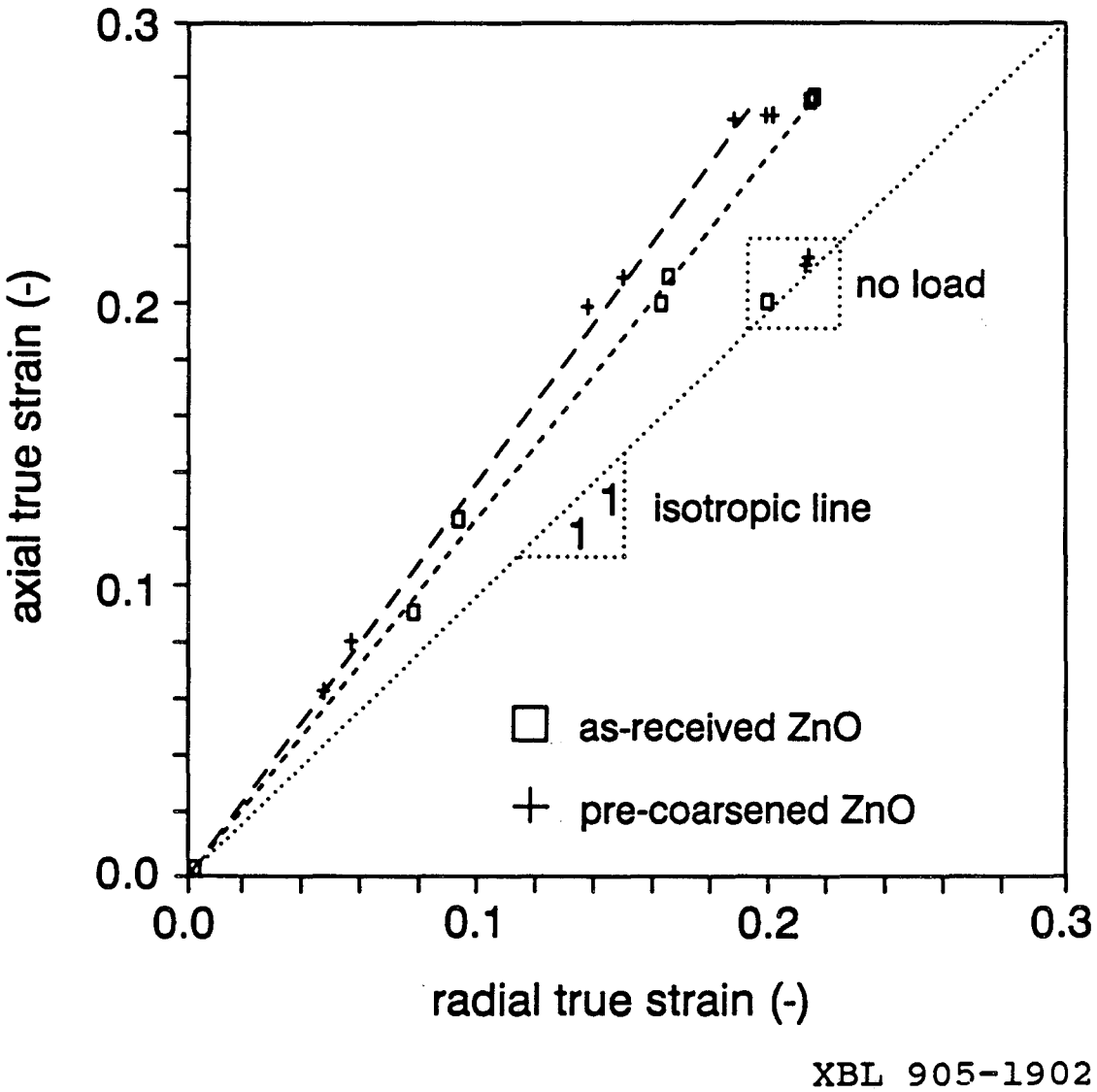
0.3
0.2
0.1
0.0
axial true strain (-)
0.0
0.1
0.2
0.3
radial true strain (-)
no load
isotropic line
1
1
as-received ZnO
pre-coarsened ZnO
XBL 905-1902

Fig. 11

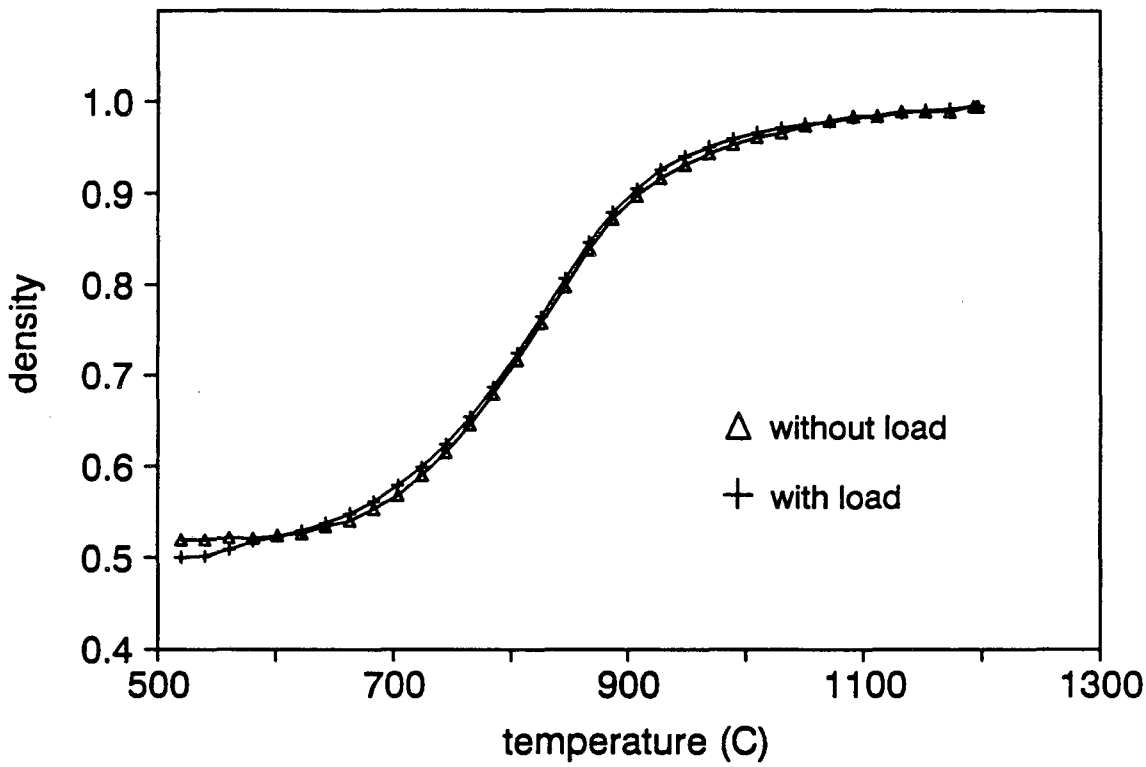

XBL 905-1903

Fig. 12

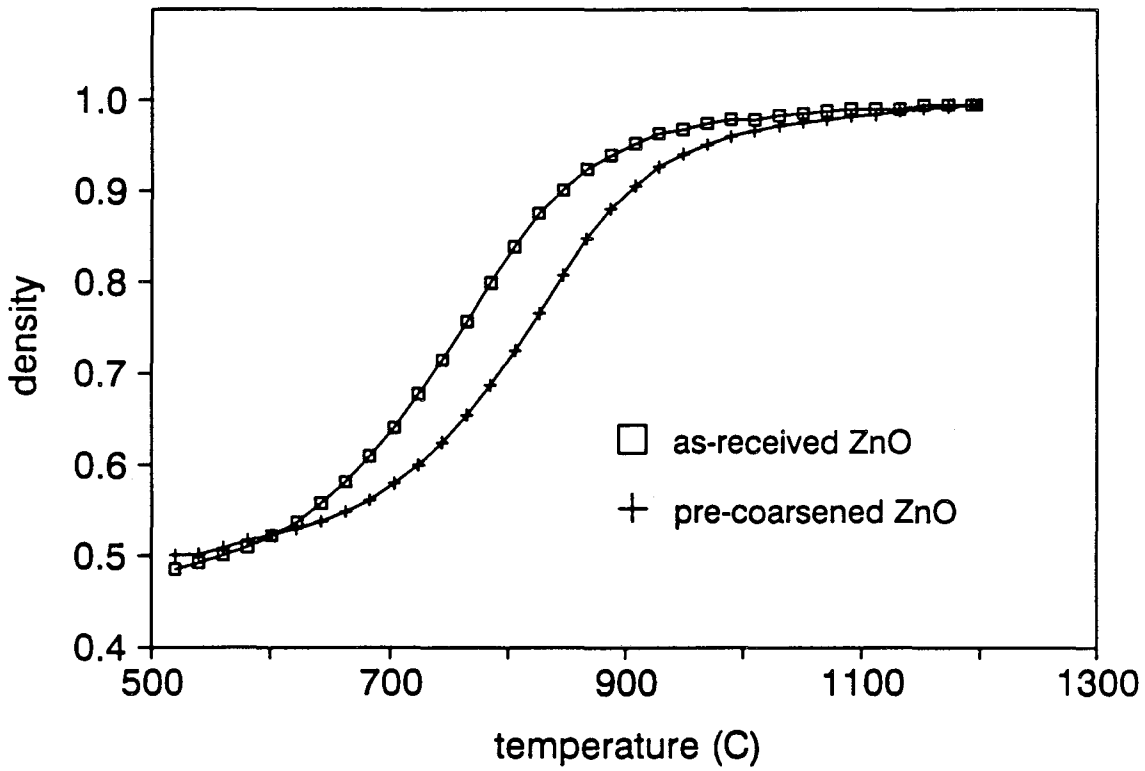

XBL 905-1904

Fig. 13

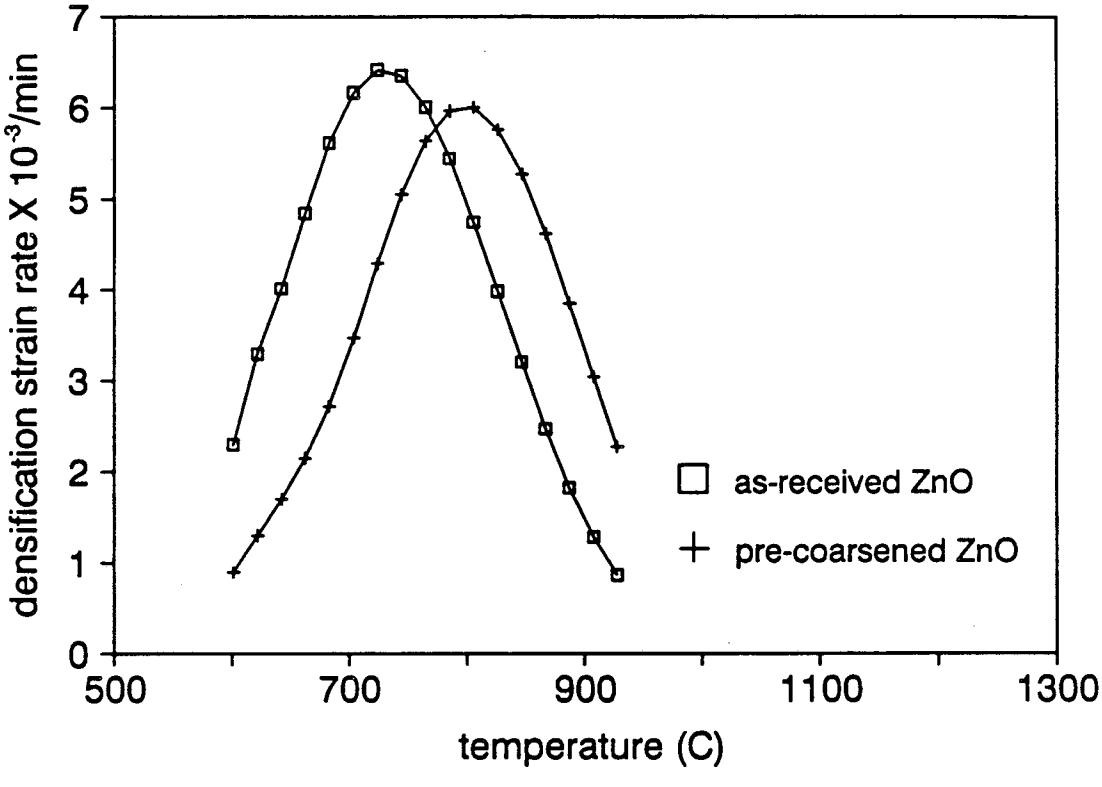
densification strain rate X 10^{-3}/min
0
1
2
3
4
5
6
7
500
700
900
1100
1300
temperature (C)
as-received ZnO
pre-coarsened ZnO
XBL 905-1905

Fig. 14

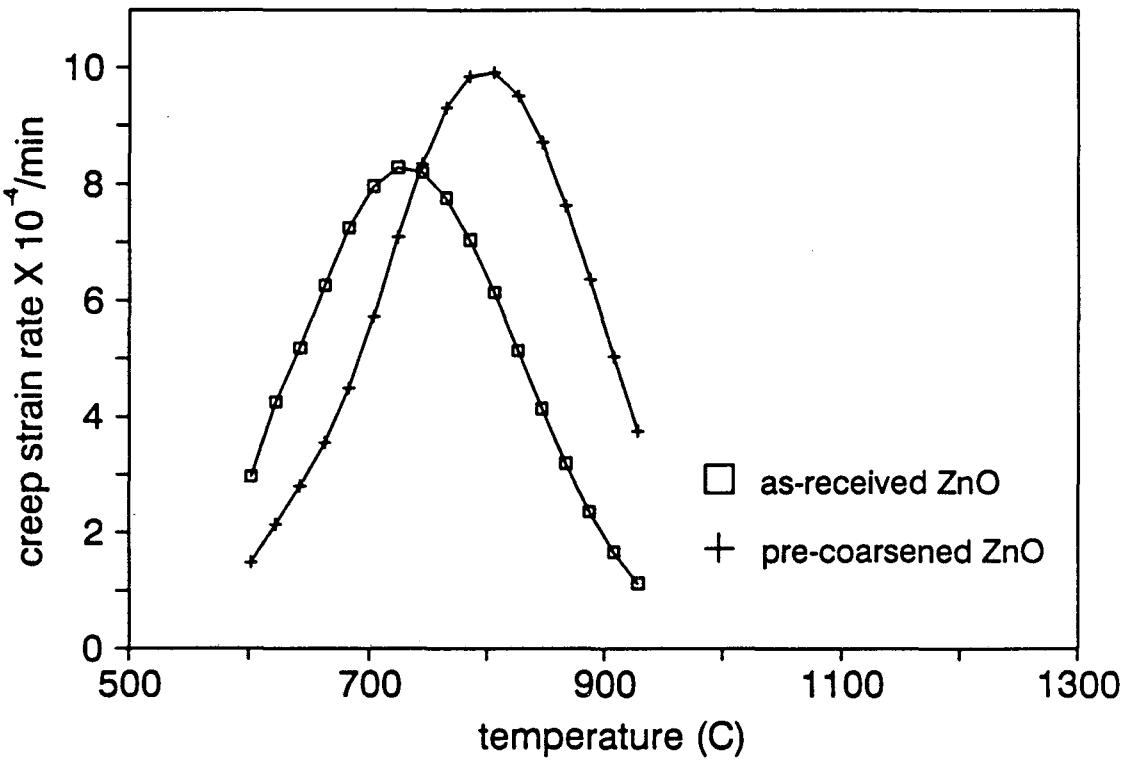

XBL 905-1906

Fig. 15

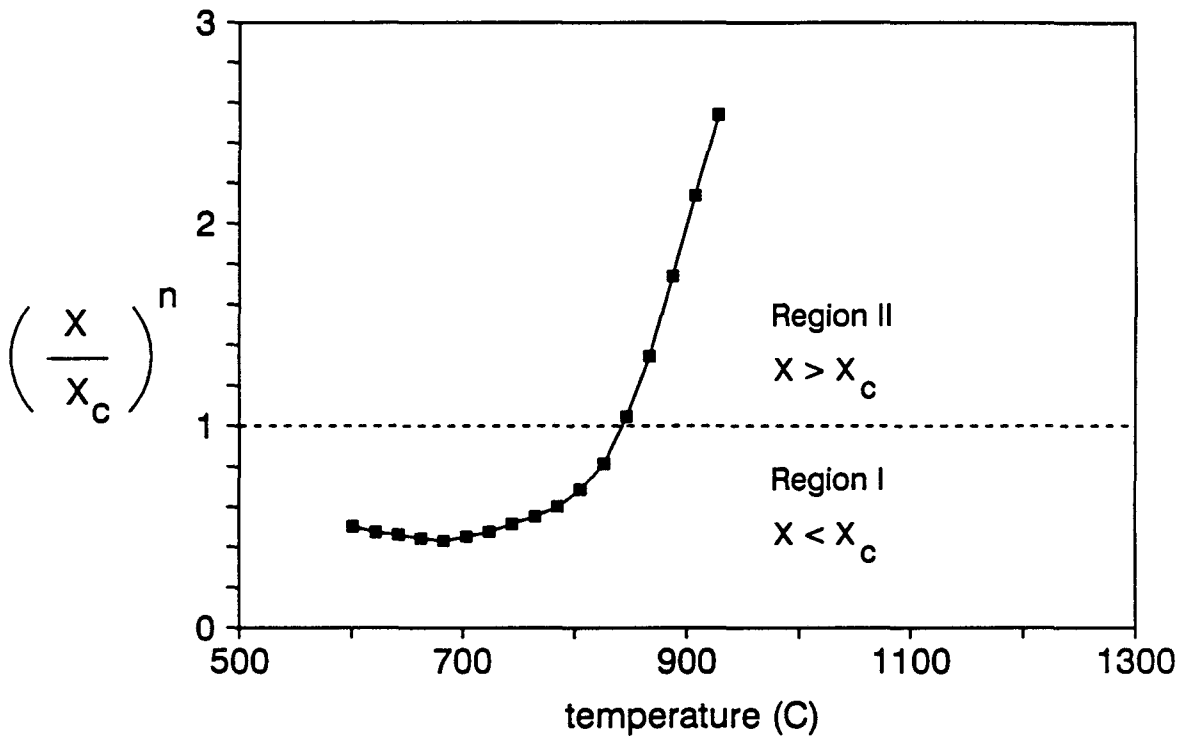

XBL 905-1907

Fig. 16

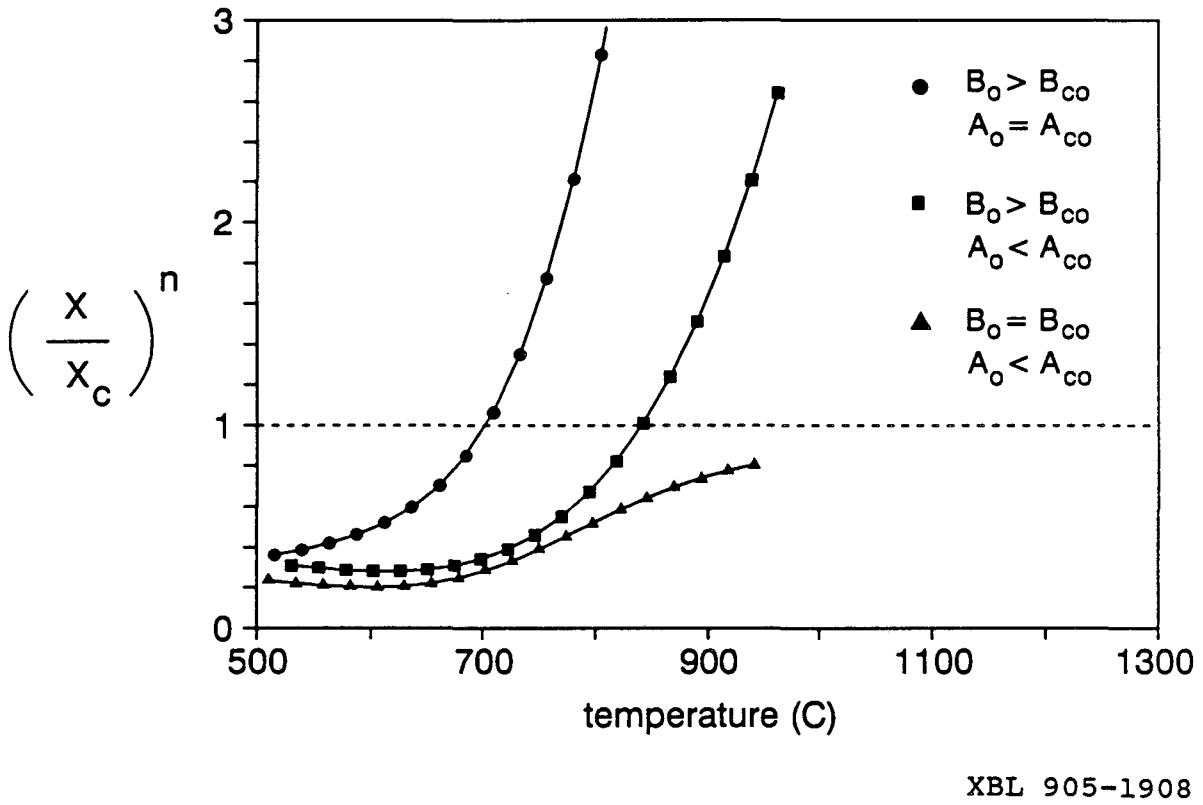
$\left(\frac{X}{X_c}\right)^n$
3
2
1
0
500
700
900
1100
1300
temperature (C)
$B_o > B_{co}$
$A_o = A_{co}$
$B_o > B_{co}$
$A_o < A_{co}$
$B_o = B_{co}$
$A_o < A_{co}$
XBL 905-1908

Fig. 17

LAWRENCE BERKELEY LABORATORY
UNIVERSITY OF CALIFORNIA
INFORMATION RESOURCES DEPARTMENT
BERKELEY, CALIFORNIA 94720